Major Groove (*S*)-α-(*N*^{6}-Adenyl)styrene Oxide Adducts in an Oligodeoxynucleotide Containing the Human *N-ras* Codon 61 Sequence: Conformations of the S(61,2) and S(61,3) Sequence Isomers from ^{1}H NMR†

Binbin Feng,‡ Markus Voehler, Liang Zhou,§ Mariella Passarelli,|| Constance M. Harris, Thomas M. Harris, and Michael P. Stone*

Center in Molecular Toxicology and Department of Chemistry, Vanderbilt University, Nashville, Tennessee 37235

Received October 23, 1995; Revised Manuscript Received January 6, 1996⊗

ABSTRACT: The (*S*)-α-(*N*^{6}-adenyl)styrene oxide adducts at positions X^6 in d(CGGACXAGAAG)·d(CTTCTTGTCCG) and X^7 in d(CGGACAXGAAG)·d(CTTCTTGTCCG), incorporating codons 60, 61 (underlined), and 62 of the human *n-ras* protooncogene, were examined by ^{1}H NMR. These were the S(61,2) and S(61,3) adducts. Chemical shift perturbations were in the 3′-direction from the sites of adduction; upfield changes associated with the styrene aromatic ring current were noted for $^{S\text{-}SO}$A^6 H2 and H1′, T^{16} N3H, H6, and CH$_3$ resonances in the S(61,2) oligomer. In the S(61,3) oligomer, $^{S\text{-}SO}$A^7 H1′, T^{16} H1′, C^{15} N4H$_a$, and H5 shifted upfield. The styrene aromatic rings flipped rapidly on the NMR time scale; under these conditions the ortho and meta aromatic protons were equivalent. A sequence effect, in which the S(61,2) adduct equilibrated between two conformers, while the S(61,3) adduct exhibited only a single conformation, was observed. Potential energy minimization of the S(61,2) adduct major conformation yielded a structure in which the styrene ring was oriented in the 3′-direction and interacted primarily with the complementary strand. For the S(61,3) adduct, 291 restraints were obtained from NOE data at three mixing times using relaxation matrix analysis. The emergent structures refined to an average rms difference of 1.3 Å, determined by pairwise analysis. These were compared to NOE intensity data; the calculated sixth root residual index was 9.2×10^{-2} at 250 ms. In the refined structure, the styrene ring was also oriented in the 3′-direction and interacted with the complementary strand. The minor conformation of the S(61,2) adduct was not identified. These results contrasted with the diastereomeric R(61,2) and R(61,3) adducts, which underwent slow ring flips on the NMR time scale and for which small sequence effects involving the minimium energy conformation of the styrene ring were observed [Feng, B., Zhou, L., Passarelli, M., Harris, C. M., Harris, T. M., & Stone, M. P. (1995) *Biochemistry 34*, 14021−14036].

Styrene is one of the top chemicals produced in the United States for the manufacture of various plastics and resins. Its toxicology (Bond, 1989) is of interest since it is mutagenic in both prokaryotes (de Meester et al., 1977; Wade et al., 1978) and eukaryotes (Bonatti et al., 1978) and possibly in humans (Ott et al., 1980; Hodgson & Jones, 1985; Matanoski & Schwarts, 1987; Wong, 1990). Styrene induces sister chromosome exchange and aberrations in human lymphocytes *in vitro* (Norppa et al., 1980, 1981). The genotoxicity is believed to be due to cytochrome P$_{450}$-mediated metabolism to styrene oxide, SO[1] (Harris et al., 1986; Foureman et al., 1989; Elovaara et al., 1991; Guengerich et al., 1991; Guengerich, 1992; Nelson et al., 1993; Nakajima et al., 1994a,b). The oxide reacts to form adducts in nucleotides, including *R* and *S* adducts at the exocyclic amino groups of guanine and adenine (Savela & Hemminki, 1986), although the distribution of DNA adducts induced *in vivo* remains uncertain.

The formation of adducts between DNA and metabolically activated chemical carcinogens, perhaps including SO, likely represents an early event in carcinogenesis (Miller, 1970, 1978). DNA adducts are generally believed to act by inducing somatic cell mutations, due to errors in replication or repair. Mutations in specific coding regions are correlated with carcinogenesis. Protooncogene coding sequences represent one set of genetic loci in which adduct-induced mutations might directly initiate cellular transformation. Mutations within a limited number of codons in the p21 gene, including codon 61, cause oncogene activation [reviewed by

† This research was supported by grants from the NIH, ES-05355 (M.P.S.) and ES-05509 (T.M.H.). Funding for the NMR spectrometer was supplied by a grant from the NIH shared instrumentation program, RR-05805, and the Vanderbilt Center in Molecular Toxicology, ES-00267. This study made use of the National Magnetic Resonance Facility at Madison, supported by NIH Grant RR-02301. NMRFAM equipment was purchased with funds from the University of Wisconsin, NSF Grants DMB-8415048 and BIR-9214394, NIH Grants RR-02301, RR-02781, and RR08438, and the USDA.

* Author to whom correspondence should be addressed.

‡ Present address: Cellular Biochemistry and Biophysics Program, Memorial Sloan-Kettering Cancer Center, New York, NY 10021.

§ Present address: Department of Pharmacology, 4 Research Court Cancer Section, Georgetown University, Rockville, MD 20850.

|| Present address: Department of Chemistry, University of Maine at Farmington, P.O. Box 976, Farmington, ME 04938.

⊗ Abstract published in *Advance ACS Abstracts,* May 1, 1996.

[1] Abbreviations: DNA, deoxyribonucleic acid; DSS, sodium 4,4-dimethyl-4-silapentanesulfonate; EDTA, ethylenediaminetetraacetic acid; HPLC, high-pressure liquid chromatography; NMR, nuclear magnetic resonance; NOE, nuclear Overhauser enhancement; NOESY, two-dimensional NOE spectroscopy; SO, styrene oxide; TPPI, time-proportional phase increment; TOCSY, total homonuclear correlated spectroscopy; 1D, one dimensional; 2D, two dimensional.

S0006-2960(95)02526-8 CCC: $12.00

Barbacid (1987)]. Hence, it seems important to understand how DNA adducts, such as styrene oxide, induce structural changes within the coding sequence at codon 61 of the *n-ras* gene.

It is not known whether SO induces mutations in codon 61 of *n-ras* or if human tumors are induced by exposure to SO, but there does exist a body of evidence suggesting chemical carcinogens do induce mutations in, and thereby activate, protooncogenes such as *ras*. This evidence comes from comparison of mutations in carcinogen-induced tumors within a number of tissues to known or suspected reaction sites of specific carcinogens [reviewed by Balmain and Brown (1988)]. It is generally believed that these tumors were induced by various chemical carcinogens. Recently, it was reported that mammary tumors previously thought to have been induced by exposure to methylnitrosourea (MNU) (Zarbl et al., 1985) actually arose from cells having preexisting mutations in *h-ras* (Cha et al., 1994), thus leaving the question unanswered as to whether MNU directly activates *h-ras* via adduct-induced mutations in the protooncogene. The latter report notwithstanding, it seems reasonable that DNA adducts located within critical coding regions of the *n-ras* protooncogene could induce activating mutations.

To address this possibility, we embarked upon studies of adduct structure within the *ras61* oligodeoxynucleotide d(CGGACAAGAAG)·d(CTTCTTGTCCG),[2] which contains the sequence for codons 60, 61 (underlined), and 62 of the human *n-ras* gene. Structural refinement of the *ras61* oligodeoxynucleotide suggested sequence-specific variations at codon 61 (Calladine, 1982) associated with the purine−pyrimidine (R-Y) step at A^4·T^{19}→C^5·G^{18} and the Y-R step at C^5·G^{18}→A^6·T^{17}; these might modulate chemical reactivity at the codon 61 site (Feng & Stone, 1995). A nonbiomimetic synthesis enabled large-scale production of site-specific (*R*)- and (*S*)-α-(*N*^{6}-adenyl)-SO-modified *ras61* oligodeoxynucleotides, while simultaneously eliminating problems in controlling the regioselectivity of adduction. The enantiomeric phenylglycinol was reacted with oligodeoxynucleotides containing 6-chloropurine deoxyriboside at either the A^6 or the A^7 nucleotide within codon 61, affording the desired diastereomer of styrene oxide at either A^6 or A^7 after subsequent deprotection and purification (Harris et al., 1991). The sequence isomers examined in this work were named the S(61,2) and S(61,3) adducts (Chart 1).

Previously, this laboratory compared solution conformations of the R(61,2) and R(61,3) adducts, obtained from ^{1}H NMR spectroscopy (Feng et al., 1995). The preferred conformation of the R(61,2) adduct was similar, but not identical, to that of the R(61,3) oligodeoxynucleotide. In both instances, structural perturbations were confined to the base pairs at and immediately adjacent to the site of adduction. In both, the styrene phenyl ring was located in the major groove and oriented toward the 5′-direction from the site of adduction. Distinct sequence-specific differences were noted. For the R(61,2) adduct, the plane of the phenyl ring was predicted to prefer an edgewise alignment in the major groove, while for the R(61,3) adduct, the preferred alignment was predicted to have the plane of the phenyl ring on the floor of the groove. The refined structures suggested greater steric hindrance in locating the styrenyl ring in the major groove adjacent to the 5′-neighbor nucleotide C^5 in the R(61,2) adduct as compared to the 5′-neighbor A^6 in the R(61,3) adduct (Feng et al., 1995). That result was correlated with *in vitro* replication studies which revealed that the R(61,2) adduct hindered replication (Latham et al., 1993).

Chart 1: (A) S(61,2) and S(61,3) Oligodeoxynucleotides, Where X Is the (*S*)-α-(*N*^{6}-Adenyl)styrene Oxide Adduct, and (B) Structure of the (*S*)-α-Styrene Oxide Adduct at Adenine N^6 and Designations of the Styrene Protons

A

ras codons

60 61 62

5′-C^1 |G^2 G^3 A^4 |C^5 X^6 A^7 |G^8 A^9 A^{10}|G^{11}-3′

3′-G^{22}|$C^{21}C^{20}T^{19}$|$G^{18}T^{17}T^{16}$|$C^{15}T^{14}T^{13}$|C^{12}-5′

ras codons

60 61 62

5′-C^1 |G^2 G^3 A^4 |C^5 A^6 X^7 |G^8 A^9 A^{10}|G^{11}-3′

3′-G^{22}|$C^{21}C^{20}T^{19}$|$G^{18}T^{17}T^{16}$|$C^{15}T^{14}T^{13}$|C^{12}-5′

B

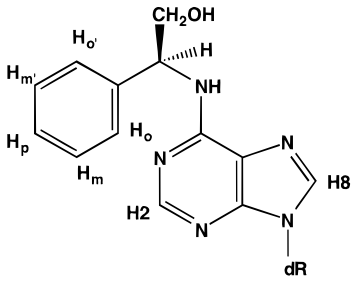

This work presents results from high-resolution ^{1}H NMR spectroscopy for the S(61,2) and S(61,3) adducts. Interproton distances from NOESY spectra are used to refine solution structures via restrained MD simulation with a simulated annealing protocol, followed by relaxation matrix back-calculation (Keepers & James, 1984; Havel & Wuthrich, 1985; Wuthrich, 1986; Nilsson et al., 1986; Borgias & James, 1990; Madrid et al., 1991; Mujeeb et al., 1993; Weisz et al., 1994). The results are compared to the unmodified *ras61* sequence (Feng & Stone, 1995) and the diastereomeric R(61,2) and the R(61,3) adducts (Feng et al., 1995). The S(61,2) and S(61,3) adducts exhibit the opposite orientation of the styrene ring in the major groove—in both *S* adducts the styrene is oriented in the 3′-direction from the lesion. A large sequence effect is also observed: the S(61,2) adduct equilibrates between two conformations on the NMR time scale, while the S(61,3) adduct exhibits a single conformation. These results extend our understanding of the dual roles that adduct stereochemistry and DNA sequence contribute toward determining the conformations of α-styrene oxide adducts at adenine N6.

MATERIALS AND METHODS

Sample Preparation. The oligodeoxynucleotide d(CTTCTTGTCCG) was purchased from the Midland Certified

[2] The oligonucleotides discussed in this paper do not have terminal phosphate groups—we abbreviate the nomenclature for oligonucleotides by leaving out the phosphodiester linkage. A, C, G, and T refer to mononucleotide units. A right superscript refers to numerical position in the oligonucleotide sequence starting from the 5′-terminus of chain A and proceeding to the 3′-terminus of chain A and then from the 5′-terminus of chain B to the 3′-terminus of chain B. C2, C5, C6, C8, C1′, C2′, etc. represent specific carbon nuclei. H2, H5, H6, H8, H1′, H2′, H2″, etc. represent the protons attached to these carbons.

Reagent Co. (Midland, TX). The concentration of the single-stranded unmodified oligodeoxynucleotide was determined from the extinction coefficient of 9.08×10^4 M^{-1} cm^{-1} at 260 nm (Borer, 1975). To construct the S(61,2) and S(61,3) α-SO-adducted duplexes, equal molar amounts of either the S(61,2) or S(61,3) strands (Harris et al., 1991), respectively, and the unmodified complementary strand were mixed in 10 mM NaH_2PO_4, 0.1 M NaCl, and 50 μM Na_2EDTA at pH 6.9. In each case, the annealed duplex was eluted from a hydroxylapatite column using sodium phosphate and desalted by gel filtration using Bio-Gel P-2 (Bio-Rad Laboratories, Richmond, CA). NMR samples were prepared in 0.1 M NaCl, 0.01 M NaH_2PO_4, and 0.05 mM Na_2EDTA (pH 7.4). For observation of nonexchangeable protons, NMR samples were repeatedly lyophilized and dissolved in 0.5 mL of 99.996% D_2O, giving a 2 mM solution. For assignments of water-exchangeable protons, samples were dissolved in a 9:1 H_2O:D_2O buffer of the same composition as described above.

NMR Spectroscopy. Spectra were recorded at ^1H frequencies of 500.13 and 750.13 MHz. The data were processed using FELIX 2.3 (Biosym Technologies, San Diego, CA), running on Iris or Indigo workstations (Silicon Graphics, Inc., Mountain View, CA). Phase-sensitive NOESY spectra in D_2O were recorded using the standard pulse sequence and the TPPI method for phase cycling; the mixing time was 250 ms. The residual water resonance was saturated during the relaxation delay and the mixing period. The NOESY pulse program was modified to eliminate artifacts from zero-quantum coherence and *zz* terms at short mixing times. A systematically shifted composite 180° pulse was implemented within the mixing period, and composite 90° pulses were used in place of the second and third 90° pulses in the standard pulse sequence (Bodenhausen et al., 1984). TOCSY experiments used the standard pulse sequence with a 100 ms MLEV-17 spinlock field (2 G). Chemical shifts were referenced internally relative to DSS. One-dimensional experiments in 90% H_2O used a 1-1 echo pulse sequence (Plateau & Gueron, 1982). Two-dimensional phase-sensitive NOESY experiments in 90% H_2O used the 1-1 sequence as the read pulse (Bax et al., 1987; Sklenar et al., 1987), at 20 °C. Convolution difference used during processing minimized the residual water signal (Marion et al., 1989). The mixing time was 250 ms.

Relaxation Matrix Analysis. For the S(61,3) duplex, NOESY experiments were run at mixing times of 150, 200, and 250 ms. Footprints were selected manually with FELIX 2.3 to fit NOE cross-peaks at the contour level which showed the weak NOEs but not random noise. For overlapped cross-peaks, footprints were estimated. NOE cross-peaks were volume integrated for the three spectra using the same contour levels. For each of the three mixing times, a hybrid intensity matrix was constructed using MARDIGRAS (Borgias & James, 1990). RMA calculations were performed on each matrix, yielding three sets of internuclear distances. The distances were averaged, and error bounds were calculated to provide the restraints used in MD calculations. Some calculated distances, primarily involving sugar protons, were not included as restraints in MD calculations since the estimated error in their measurement exceeded the range of distances physically possible between the two protons in the covalent structure of the oligodeoxynucleotide. Individual distance restraints calculated by MARDIGRAS to be greater than 5 Å were removed from the distance restraint set. Additional restraints were removed if they were found to be inconsistent with a reasonable structure. In general, these difficulties were due to errors in intensity measurements arising from spectral overlap or from cross-peaks close to the water resonance whose intensities were altered by the water presaturation pulse used during acquisition of NOESY spectra. An isotropic correlation time τ_c of 5 ns was used for both sugar and base protons (Zegar et al., 1996).

Restrained Molecular Dynamics. INSIGHTII (Biosym Technologies, San Diego, CA) was used to build starting structures and for molecular visualization. Potential energy minimization and MD calculations were performed using X-PLOR (Brunger, 1992). The empirical energy function derived from the CHARMM force field (Brooks et al., 1983) and developed for nucleic acids treated hydrogens explicitly (Nilsson & Karplus, 1986). The nonbonded interactions included van der Waals and electrostatic terms, which used the pure Lennard-Jones and Coulomb functions, respectively. The electrostatic term was based on a reduced charge set of partial charges (−0.32/residue) and a dielectric constant of 4.0. The cutoff radius for nonbonded interactions was 11 Å, and the nonbonded list was updated if any atom moved more than 0.5 Å. The SHAKE algorithm (Ryckaert et al., 1977) fixed bond lengths involving hydrogens. The integration time step in the molecular dynamics calculations was 1 fs. Structure coordinates were archived every 0.1 ps. Back-calculation of NMR data was performed using CORMA (Keepers & James, 1984). The refined structures were analyzed using DIALS AND WINDOWS 1.0 (Ravishankar et al., 1989).

RESULTS

UV Melting Studies. In comparison to the S(61,3) adduct and the previously studied R(61,2) and R(61,3) adducts (Feng et al., 1995), the S(61,2) adduct was the least stable. The first derivative of the melting curve indicated the melting temperature (T_m) of the S(61,2) adduct to be 37 ± 1 °C, a 16 °C decrease compared to the unmodified *ras61* oligomer. The first derivative of the S(61,3) melting curve indicated T_m to be 42 ± 1 °C, close to the melting temperatures of the R(61,2) and R(61,3) adducts and 11 °C lower than the unmodified *ras61* sequence.

Spectral Assignments. Both modified oligodeoxynucleotides shared a number of spectral features. C^5 H5 and H6 shifted upfield as compared to the remainder of the cytosine H5 and H6 protons, presumably due to increased stacking interactions since C^5 was flanked on both sides by adenine. C^{12} H5 and H6, from the terminal C·G base pair, were located downfield of the remainder of the cytosine H5 and H6 protons, which were clustered at 5.4−5.7 and 7.3−7.5 ppm, respectively. This resulted in the overlap of a number of cross-peaks. For the S(61,2) adduct, C^1, T^{14}, T^{17}, C^{20}, and C^{21} H6 and G^{11} H8 were superimposed. Likewise, C^1, G^3, C^5, and T^{17} H1′ were superimposed, as were A^7, A^9, A^{10}, G^{18}, and T^{19} H1′ and A^4, T^{13}, T^{14}, T^{16}, and G^{22} H1′. For the S(61,3) adduct, C^1, T^{13}, T^{14}, C^{15}, T^{17}, C^{20}, and C^{21} H6 and G^8 and G^{11} H8 were superimposed. A^6, A^{10}, G^{11}, T^{14}, G^{18}, and T^{19} H1′ were superimposed, as were A^4, T^{13}, and G^{22} H1′.

(a) Nonexchangeable Protons of the S(61,2) Adduct. The notable feature of the S(61,2) adduct was the presence of a minor conformation in slow exchange with the predominant

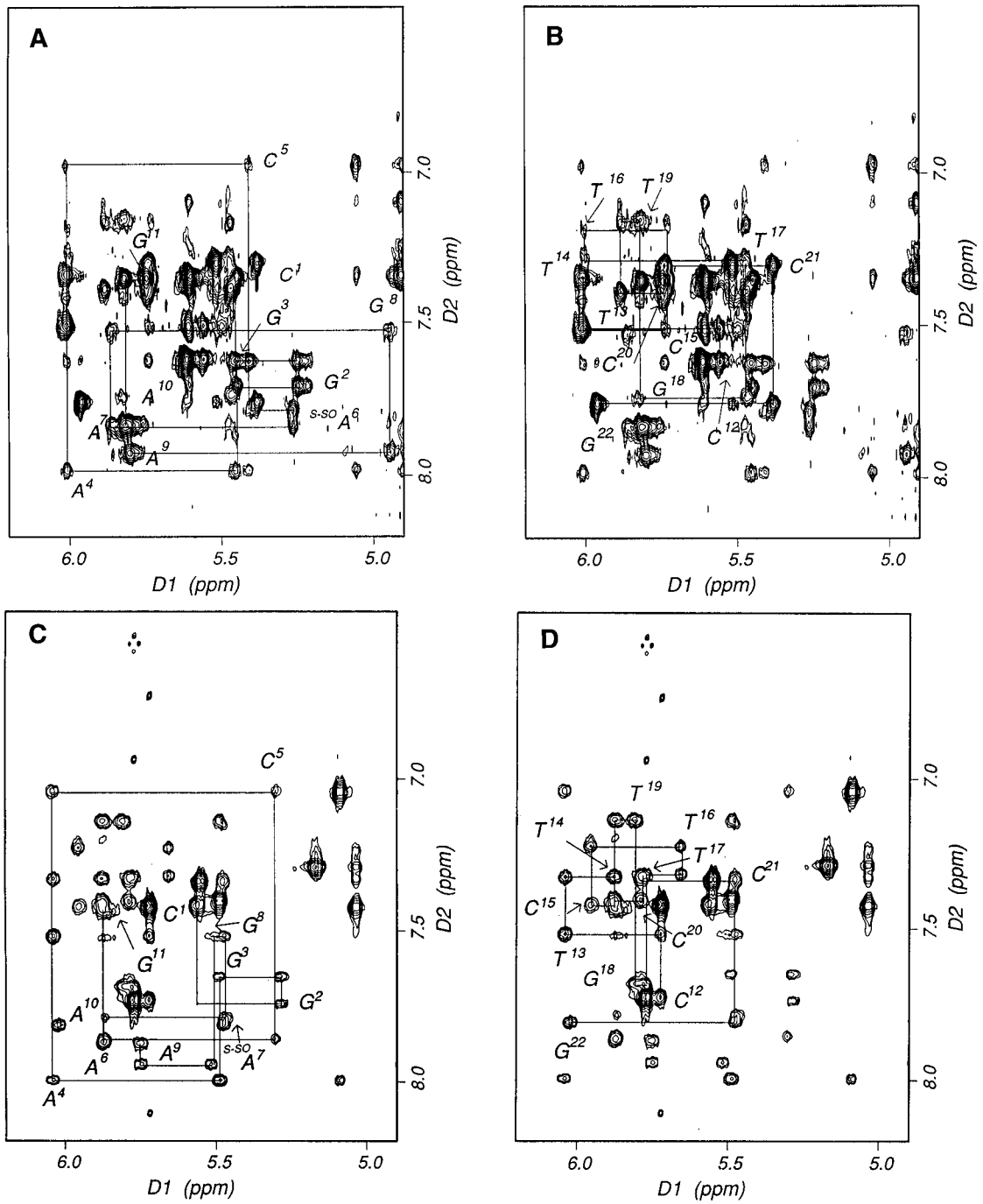

FIGURE 1: Expanded plots of phase-sensitive NOESY spectra at 250 ms mixing time showing the sequential NOE connectivities from the aromatic to H1′ protons. (A) Sequential NOE connectivities for nucleotides $C^1 \rightarrow G^{11}$ for the major conformation of the S(61,2) adduct, recorded at 750 MHz. (B) Sequential NOE connectivities for nucleotides $C^{12} \rightarrow G^{22}$ for the major conformation of the S(61,2) adduct, recorded at 750 MHz. (C) Sequential NOE connectivities for nucleotides $C^1 \rightarrow G^{11}$ for the S(61,3) adduct. (D) Sequential NOE connectivities for nucleotides $C^{12} \rightarrow G^{22}$ for the S(61,3) adduct. The base positions are indicated at the intranucleotide aromatic-to-sugar H1′ NOE cross-peak.

conformation.[3] Figure 1A,B shows base-to-H1′ connectivities, at a mixing time of 250 ms and at 10 °C. At higher temperatures, cross-peaks broadened. From data obtained at a ^{1}H frequency of 750 MHz, assignments for the major conformation were made in the base-to-H1′ and base-to-H2′/H2″ regions for both the modified and complementary strands. In the modified strand sequential connectivities between nucleotides $G^3 \rightarrow A^4 \rightarrow C^5 \rightarrow {}^{S\text{-}SO}A^6 \rightarrow A^7 \rightarrow G^8$ were weak. In the complementary strand connectivities between $C^{15} \rightarrow T^{16} \rightarrow T^{17} \rightarrow G^{18} \rightarrow T^{19}$ were weak. One difference between the S(61,2) adduct and the unmodified *ras61* oligodeoxynucleotide was a 0.2 ppm upfield shift of ${}^{S\text{-}SO}A^6$ H8. Table S1 in the Supporting Information lists the chemical shifts of the nonexchangeable protons for the major conformation.

(b) Nonexchangeable Protons of the S(61,3) Adduct. Figure 1C,D shows the base-to-H1′ connectivities from spectra collected at 20 °C. As compared to the S(61,2)

[3] Two samples of the S(61,2) adduct were independently synthesized. Both showed the same behavior, discounting the possibility that there was a sample impurity. The identity of the minor conformation was not established but was estimated to be present in the approximate ratio of 7:3 major:minor by spectral integration.

adduct, the signals were sharp and well resolved. In both strands, a complete set of sequential connectivities was observed. One difference between the S(61,3) adduct and the S(61,2) adduct was the upfield shift of $^{S\text{-}SO}A^7$ H8. Whereas in the S(61,2) adduct A^7 H8 was downfield of $^{S\text{-}SO}A^6$ H8, in the S(61,3) adduct, $^{S\text{-}SO}A^7$ H8 was upfield of A^6 H8. A large downfield shift was noted for G^8 H1′. Other notable features were upfield shifts of C^{15} H5 and H6 as compared to the unmodified *ras61* sequence, an upfield shift of T^{14} H1′, a downfield shift of C^{15} H1′, and an upfield shift of T^{16} H1′. Table S2 in the Supporting Information lists the chemical shifts of the nonexchangeable protons.

(c) Exchangeable Protons. For both modified oligodeoxynucleotides, the imino resonances from the terminal base pairs C^1•G^{22} and G^{11}•C^{12} were missing, due to exchange broadening. T^{13} N3H was also typically exchange broadened under most conditions. Similar to the nonexchangeable protons (Figure 2A,B), the exchangeable protons of the S(61,2) oligomer also exhibited signs of conformational exchange, whereas a single conformation was observed for the S(61,3) oligomer (Figure 2C). The chemical shifts of the exchangeable protons for both oligodeoxynucleotides are listed in Tables S3 and S4 in the Supporting Information.

The S(61,2) Oligomer. Assignments of the exchangeable imino and amino protons (Boelens et al., 1985) from the major conformation were made from 750 MHz NOESY spectra measured at 5 °C and a mixing time of 250 ms, shown in Figure 2A,B. These were complicated by conformational exchange for the imino protons of G^8, T^{16}, T^{17}, G^{18}, and T^{19}. T^{16} N3H was broadened and shifted 0.72 ppm upfield from its position in the unmodified *ras61* oligomer, and it appeared as a downfield shoulder under the G^2 N1H resonance. No NOE was observed between the T^{16} and T^{17} N3H resonances. T^{17} N3H, at 13.6 ppm, exhibited a cross-peak with a resonance at 6.82 ppm, which was assigned to $^{S\text{-}SO}A^6$ H2. C^5 $N4H_{a,b}$ shifted downfield by 0.31 and 0.12 ppm, respectively.

The S(61,3) Oligomer. Assignments were made from NOESY spectra measured at 20 °C (Boelens et al., 1985). The assignment of the imino proton region of the ^{1}H NMR spectrum is shown in Figure 2C. The spectrum was similar to that observed for the unmodified *ras61* oligomer; 8 of the 11 imino resonances were observed under these conditions. As compared to the unmodified *ras61* oligodeoxynucleotide, a 0.1 ppm upfield chemical shift for G^8 N1H was observed. T^{16} N3H overlapped T^{14} N3H, while T^{17} and T^{19} N3H overlapped. A notable feature of the spectrum was the substantial upfield chemical shift of C^{15} $N4H_a$, which was observed at 4.19 ppm. This unusual assignment was based upon observation of NOEs between C^{15} $N4H_a$ and C^{15} $N4H_b$, observed at 8.06 ppm, and G^8 N1H, observed at 12.2 ppm. The large upfield shift was presumed to be due to ring-current shielding of the adjacent styrene ring. A chemical shift of similar magnitude, induced by the styrene ring current, was observed for the R(61,2) SO-adducted oligomer (Feng et al., 1995).

(d) Styrene Protons. The S(61,2) Oligomer. A TOCSY spectrum showing the styrene aromatic protons is shown in Figure 3A. Three resonances were observed, located at δ 7.10, 7.25, and 7.34 ppm, respectively. The δ 7.10, 7.25 ppm cross-peak was not observed in a DQF-COSY experiment (Figure 3B). It was observed in the NOESY spectrum (Figure 3C), and it had a different phase from ROE peaks

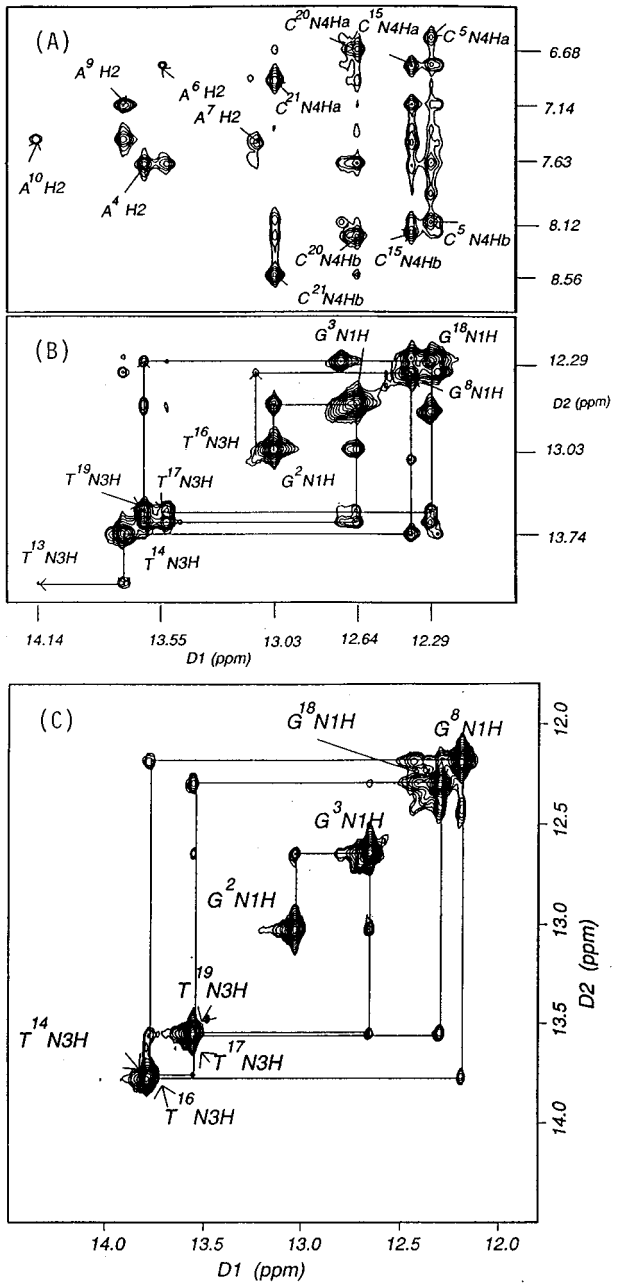

FIGURE 2: Expanded plot of a phase-sensitive NOESY spectrum for the S(61,2) adduct at 250 ms mixing time showing (A) NOE connectivities between imino−amino protons and imino−H2 of base pairs G^2•C^{21}→A^{10}•T^{13} and (B) sequential NOE connectivities for the imino protons. The data were recorded at 750 MHz at 5 °C. (C) Expanded plot of a phase-sensitive NOESY spectrum for the S(61,3) adduct at 250 ms mixing time showing the sequential NOE connectivities for the imino protons of base pairs G^2•C^{21}→A^{10}•T^{13}.

in a ROESY experiment (Figure 3D). It was assigned as an exchange peak. Therefore, the ^{1}H resonances of the styrenyl ring were observed as two signals at 7.10 and 7.34 ppm. The two ortho protons, H_o and $H_{o'}$, were superimposed at 7.34 ppm, identified from the NOESY spectrum in which they exhibited a strong cross-peak to the benzylic proton H_b at 4.91 ppm. The two meta protons, $H_{m,m'}$, and the para proton, H_p, were overlapped at 7.10 ppm. H_b was identified both from the TOCSY and from the NOESY spectrum by virtue of a strong cross-peak to $H_{\beta',\beta''}$ of the CH_2OH group. The latter protons were located at δ 3.49 ppm.

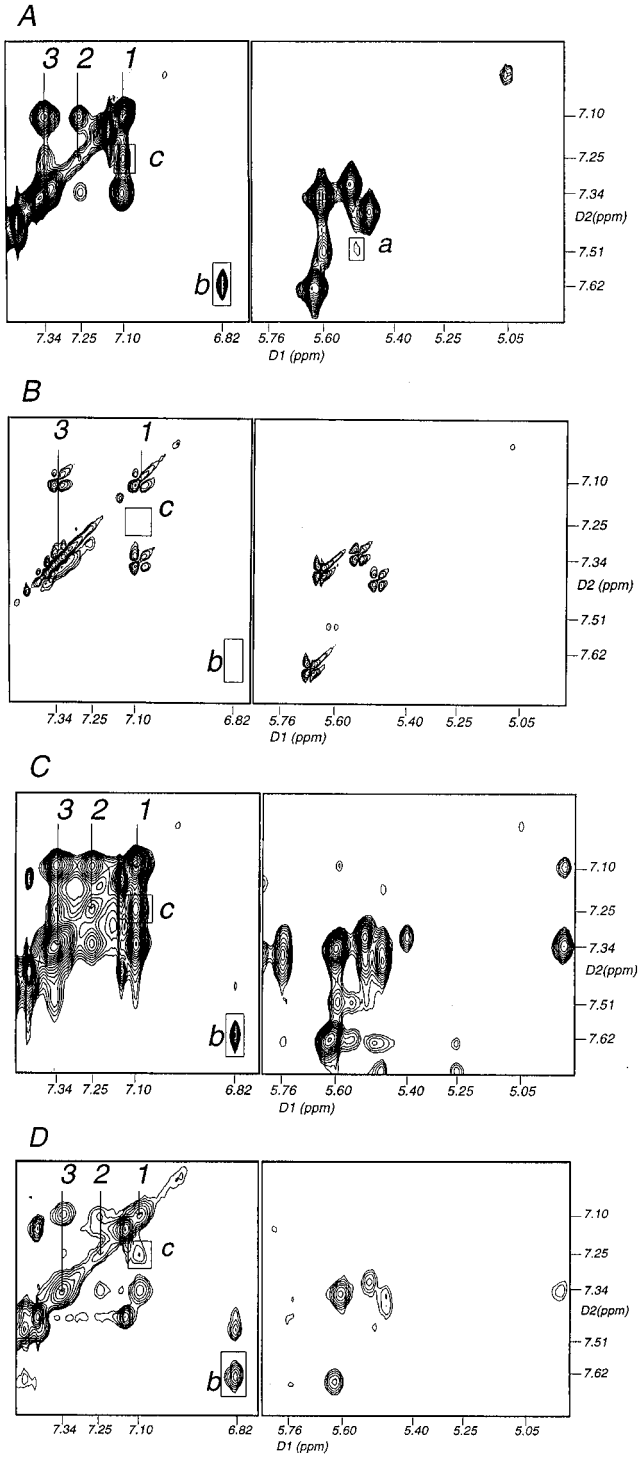

FIGURE 3: Expanded plots for the S(61,2) adduct, showing the styrene aromatic resonances and evidence of conformational exchange. (A) TOCSY spectrum. Three putative styrene aromatic resonances were observed, labeled as diagonal resonances 1−3. (B) DQF-COSY spectrum. Cross-peaks a (weak in TOCSY data), b, and c were not observed. (C) NOESY spectrum at 250 ms mixing time. Cross-peaks b and c were observed. (D) ROESY spectrum. Cross-peaks b and c were observed, with opposite phase. The data were recorded at 10 °C.

The S(61,3) Oligomer. The styrene aromatic resonances were not resolved. The five aromatic protons of the styrene ring were observed as two signals of area 4:1 at δ 7.29 and 7.23 ppm. The integral at δ 7.23 ppm had an area of 2, overlapped with T^{16} H6. The observation of a strong NOE between H_b and the signal of area 4 established that H_o and $H_{o'}$ must be isochronous or nearly so. The resonance at 7.23 ppm was assigned to H_p since an NOE was observed between this proton and T^{14} CH_3, and a weak NOE was observed between this proton and H_b. H_b located at 5.17 ppm was identified both from the TOCSY and from the NOESY spectrum by virtue of a strong cross-peak to $H_{\beta',\beta''}$ of the CH_2OH group. The latter protons were located at δ 3.42 and 3.71 ppm and exhibited strong coupling.

Styrene Oxide−DNA NOE Connectivities. The S(61,2) Adduct. NOEs between the major conformation and the DNA involved major groove protons and were oriented in the 3′-direction from the site of the lesion (Figure 4). The $H_{o,o'}$ and $H_{m,m',p}$ resonances showed NOEs to C^{15} H5 and H6. These styrene resonances also showed cross-strand NOEs to T^{16} CH_3, and to T^{17} CH_3, base-paired to $^{S\text{-}SO}A^6$. There were also NOEs observed between styrene oxide and exchangeable protons of DNA. The $H_{o,o'}$ and $H_{m,m',p}$ resonances showed NOEs to T^{17} N3H and to C^{15} $N4H_{a,b}$. In the 5′-direction, NOEs were observed between H_b and the CH_2OH protons of styrene and DNA. H_b showed NOEs to C^5 H5 and H6, as did the methylenic protons. H_b showed NOEs to C^5 $N4H_{a,b}$, as did $H_{\beta',\beta''}$. At 250 ms mixing time, both first-order and higher order (spin diffusion) NOEs were observed. The $H_{o,o'}$ and $H_{m,m',p}$ resonances showed NOEs to C^5 H5, H6, and $N4H_a$ believed to be due to spin diffusion, via H_b and $H_{\beta',\beta''}$. $H_{\beta',\beta''}$ showed a NOE to T^{16} CH_3, also believed due to spin diffusion. These disappeared when the spectrum was recorded with the shorter mixing time of 100 ms.

The S(61,3) Adduct. NOE connectivities involved major groove protons (Figure 5). At the lesion site, the $H_{o,o',m,m'}$ resonance showed an NOE to T^{16} CH_3, while H_b showed an NOE to $^{S\text{-}SO}A^7$ N6H. For the styrene aromatic protons, additional NOEs to DNA protons were oriented in the 3′-direction from the site of the lesion. The $H_{o,o',m,m'}$ resonance showed NOEs to C^{15} H_5 and G^8 N1H. Both the H_p and $H_{o,o',m,m'}$ resonances showed NOEs to T^{14} CH_3. H_p also showed an NOE to C^{15} H5. The methylenic protons of the CH_2OH group showed NOEs to $^{S\text{-}SO}A^7$ N6H. Both the H_p and $H_{o,o',m,m'}$ resonances showed NOEs to C^{15} $N4H_{a,b}$. H_b showed an additonal NOE in the 5′-direction, to A^6H8.

Restrained Molecular Dynamics for the S(61,3) Adduct. The rapid rotation of the styrene ring in the S(61,3) adduct complicated the estimation of interproton distances at and next to the lesion site, since NOEs observed between the ortho and meta protons represented time-averaged values over o, o′ and m, m′ positions. The assumption was made that the observed NOE resulted from only one (i.e., o or o′, m or m′) position. The assignment of specific NOEs to o, o′, m, or m′ was made by inspection of the IniB structure built with the SO phenyl ring oriented in the 3′-direction from $^{S\text{-}SO}A^7$. Consequently, the styrene−DNA restraints were less defined, and larger bounds were placed on them.

The final restraints consisted of 291 of the original 348 distances calculated by MARDIGRAS. Excluding the terminal base pairs, an average of 27 intranucleotide, internucleotide, and empirical distances were obtained for each base pair. Eight of these were estimated distances between styrene aromatic protons and DNA protons or distances involving water-exchangeable protons, which were not derived by MARDIGRAS calculations. The NOE distance restraints were separated into four sets. Class 1 consisted of the 164 best distance restraints, class 2 contained 65 restraints, class 3 contained 18 restraints, and class 4

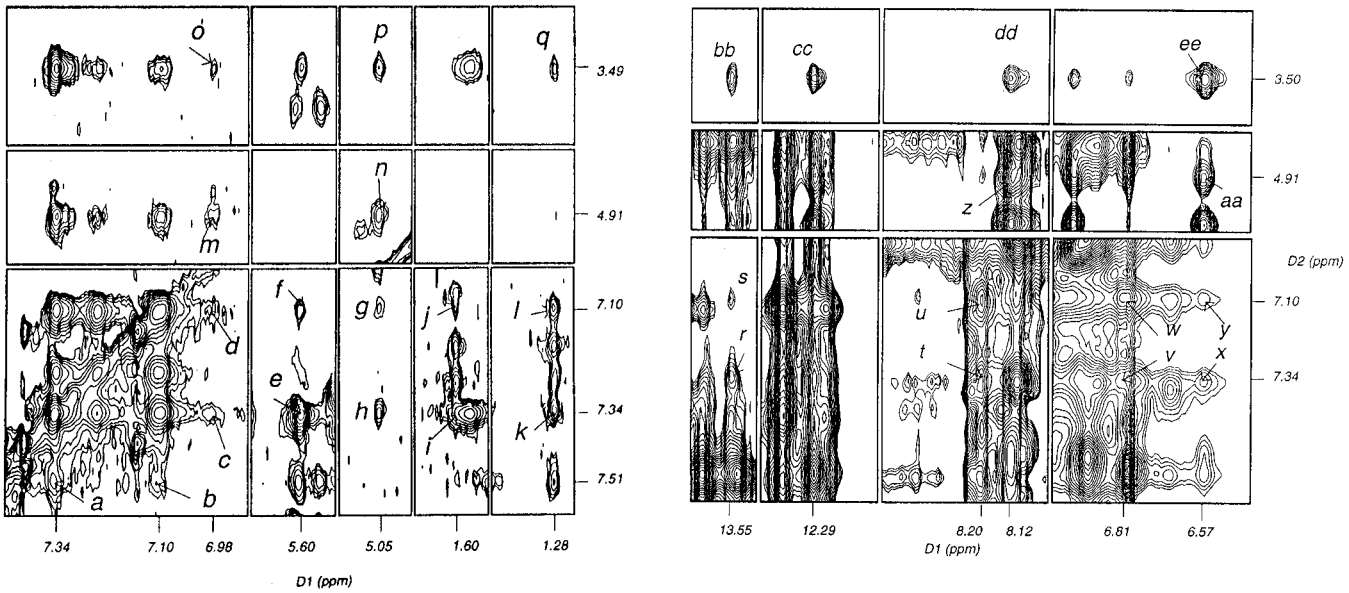

FIGURE 4: NOEs observed between SO and DNA in the S(61,2) duplex: a, C^{15} H6→$H_{o,o'}$; b, C^{15} H6→$H_{m,m',p}$; c, C^{5} H6→$H_{o,o'}$; d, C^{5} H6→$H_{m,m',p}$; e, C^{15} H5→$H_{o,o'}$; f, C^{15} H5→$H_{m,m',p}$; g, C^{5} H5→$H_{m,m',p}$; h, C^{5} H5→$H_{o,o'}$; i, T^{17} CH_3→$H_{o,o'}$; j, T^{17} CH_3→$H_{mm',p}$; k, T^{16} CH_3→$H_{o,o'}$; l, T^{16} CH_3→$H_{m,m',p}$; m, C^{5} H6→H_b; n, C^{5} H5→H_b; o, C^{5} H6→$H_{\beta',\beta''}$; p, C^{5} H5→$H_{\beta',\beta''}$; q, T^{16} CH_3→$H_{\beta',\beta''}$; r, T^{17} N3H→$H_{o,o'}$; s, T^{17} N3H→$H_{m,m',p}$; t, C^{15} $N4H_b$→$H_{o,o'}$; u, C^{15} $N4H_b$→$H_{m,m',p}$; v, C^{15} $N4H_a$→$H_{o,o'}$; w, C^{15} $N4H_a$→$H_{m,m',p}$; x, C^{5} $N4H_a$→$H_{o,o'}$; y, C^{5} $N4H_a$→$H_{m,m',p}$; z, C^{5} $N4H_b$→H_b; aa, C^{5} $N4H_a$→H_b; bb, T^{17} N3H→$H_{\beta',\beta''}$; cc, G^{18} N1H→$H_{\beta'\beta''}$; dd, C^{5} $N4H_b$→$H_{\beta',\beta''}$; ee, C^{5} $N4H_a$→$H_{\beta',\beta''}$.

consisted of the 44 worst restraints. The distribution of experimental restraints is collected in Table 1. The complete set of experimental and empirical restraints is collected in Table S5 in the Supporting Information.

The superpositions of five MD structures starting from either IniA or IniB are shown in Figure 6A,B. Figure 6C shows the superposition of the average MD structures emergent from either IniA or IniB. The sets of five structures calculated from IniA and IniB converged to similar structures, which resembled B-DNA. The positions of the atoms in the phosphodiester backbone were less certain than were the positions of the nucleotide bases, reflecting the lack of experimental restraints to define the backbone atoms. The terminal base pairs were also less well refined in the structures emergent from the MD calculations.

The precision of the emergent structures was monitored by pairwise measurements of rms deviations, the results of which are shown in Figure 7. Figure 7A confirms the large difference between the starting structures IniA and IniB, on the order of 6 Å rmsd. Figure 7B,C reveals that the structure emergent from the calculations was closer to IniB than to IniA, indicating that the MD calculations resulted in the convergence of the IniA structure toward a B-like final structure. Figure 7D shows the pairwise comparison of the emergent structures from the MD calculations. The average rmsd was 1.3 Å, with the maximum rmsd (between the two most differing structures) measured as 1.7 Å. Thus, the structural refinement defined a family of closely related structures with reasonable precision. The 10 MD structures were averaged and energy minimized to obtain the final rMD structure shown in Figure 8.

Complete Relaxation Matrix Calculations for the S(61,3) Adduct. Table 2 shows *R*-factors calculated for the starting structures and the rMD structures, calculated at three values of the NOE mixing time. Consistent results were obtained at each of the three mixing times, with the best values being observed for the 250 ms data. This reflected the improved sensitivity of the longer mixing time data. At 250 ms, the *R*-factor for IniB was 11.4×10^{-2} as compared to a value of 16.4×10^{-2} for IniA. The *R*-factor decreased when the starting structures IniA and IniB were compared to the structures rMDA and rMDB which emerged from the calculations. As compared to the two starting structures, which exhibited different *R*-factors, the values calculated for the emergent rMDA and rMDB structures were 9.4×10^{-2} at 250 ms. The refined family of structures was in reasonable agreement with the available NOE-based restraints.

Potential Energy Minimization of the Major Conformation of the S(61,2) Adduct. The conformational exchange of this adduct prevented the use of NOE restraints in molecular dynamics structural refinement. Figure 9 shows the structure derived by potential energy minimization (PEM) starting from the phenyl moiety of styrene oriented on the 3′-side of the modified site, consistent with the observed pattern of NOEs for the major conformation. The SO adduct occupied the major groove of the DNA between C^5•G^{18} and A^7•T^{16} base pairs and was oriented in the 3′-direction from the site of attachment at $^{S\text{-}SO}A^6$, as predicted. Because PEM calculations are strongly dependent upon choice of starting structure, the calculations were repeated using a different starting structure having the phenyl moiety oriented on the 5′-side of the modified site. Under these conditions, in the final minimized structures, the styrene phenyl ring was also facing toward the 3′-side of the SO lesion.

DISCUSSION

Interest in SO adduct structure within the *n-ras* proto-oncogene stems from the observation that mutagenesis at codon 61 leads to oncogene activation. Previous work with (*R*)-α-(N^6-adenyl)styrene oxide adducts compared the R(61,2) with the R(61,3) adduct and demonstrated discernible sequence-specific alterations in adduct structure within the *ras61* oligodeoxynucleotide (Feng et al., 1995). These may correlate with differences in DNA replication for the R(61,2) and R(61,3) adducts (Latham et al., 1993, 1995; Latham & Lloyd, 1994). The present studies of the S(61,2)- and

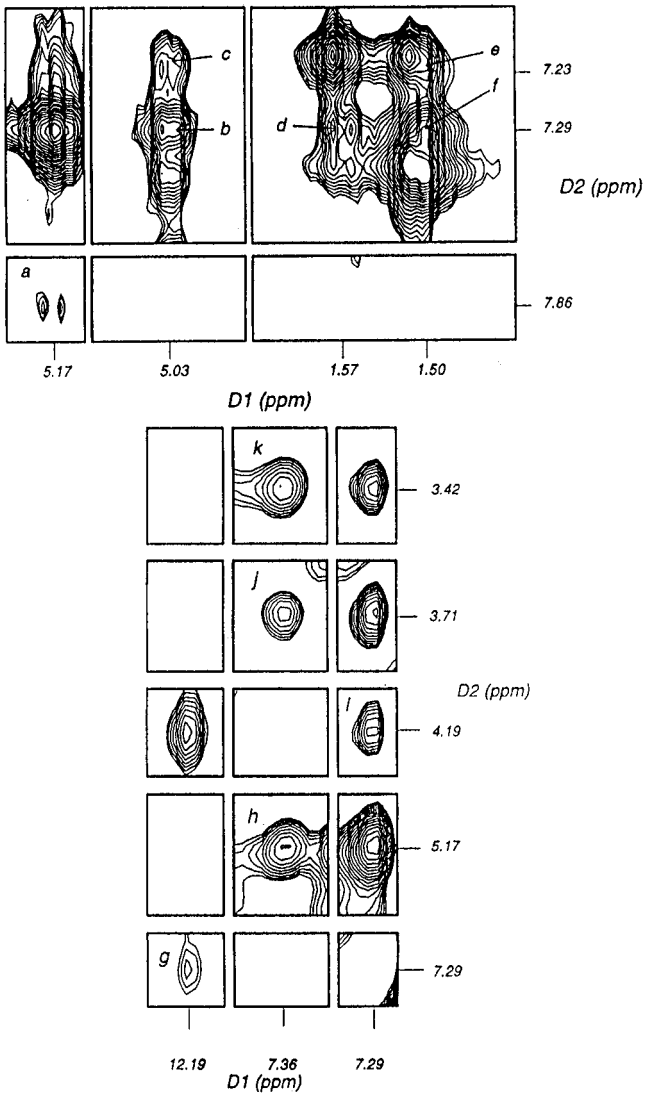

FIGURE 5: NOEs observed between SO and DNA in the S(61,3) duplex: a, A^6 H8→H_b; b, C^{15} H5→$H_{o,o',m,m'}$; c, C^{15} H5→H_p; d, T^{16} CH_3→$H_{o,o',m,m'}$; e, T^{14} CH_3→H_p; f, T^{14} CH_3→$H_{o,o',m,m'}$; g, G^8 N1H→$H_{o,o',m,m'}$; h, $^{S\text{-}SO}A^7$ N6H→H_b; i; C^{15} N4H_a→$H_{o,o',m,m'}$; j, $^{S\text{-}SO}A^7$ N6H→$H_{\beta'}$; k, $^{S\text{-}SO}A^7$ N6H→$H_{\beta''}$.

S(61,3)-α-styrene oxide adducts extend upon the previous work with the *R* diastereomers. They illustrate the role of DNA sequence in modulating adduct conformation. While the S(61,2) adduct equilibrates between two conformations, moving the (*S*)-α-styrene oxide lesion one nucleotide downstream results in an 5 °C increase in T_m and the observation of a single major groove conformation.

Oligodeoxynucleotide Conformation. The conformational interchange of the S(61,2) adduct notwithstanding, the significant feature observed for both the PEM-calculated major conformation of the S(61,2) adduct and the NOE-refined structure of the S(61,3) adduct was the facile accommodation of both within the major groove and the orientation of both in the 3′-direction from the respective lesion sites. The lack of steric hindrance was evidenced by the rapid flipping of the styrene aromatic ring in each instance. Figure 10 details stacking patterns at the lesion sites for each of these adducts and suggests that, in both instances, these adducts did not substantially alter base-pairing geometry at the lesion site. This result contrasted with previous studies on the corresponding sequence isomeric R(61,2) and R(61,3) adducts, in which the styrene rings interfered sterically with the 5′-neighbor base pairs. In that case, for the R(61,2) adduct in which the 5′-neighbor was cytosine, the 5′-neighbor C·G base pair was displaced toward the minor groove to accommodate the styrene ring (Feng et al., 1995).

Table 1: Distribution of Experimental Restraints among Nucleotide Units of the S(61,3) Adduct[a]

nucleotide	intranucleotide restraints	internucleotide restraints[b]	total exptl restraints
C^1	12	0	12
G^2	8	4	12
G^3	8	3	11
A^4	10	3	13
C^5	12	7	19
A^6	9	4	13
X^7	5	4	9
G^8	10	3	13
A^9	9	4	13
A^{10}	9	5	14
G^{11}	9	5	14
C^{12}	8	0	8
T^{13}	5	9	14
T^{14}	4	6	10
C^{15}	5	6	11
T^{16}	9	7	16
T^{17}	7	8	15
G^{18}	7	4	11
T^{19}	10	10	20
C^{20}	7	7	14
C^{21}	6	6	12
G^{22}	9	4	13

[a] Eleven styrene−DNA and styrene−styrene NOEs and one cross-strand NOE between T^{19} and A^4 are not included in the table. [b] The internucleotide NOEs are listed in the direction $n \rightarrow n - 1$.

NOEs between the phenyl moiety and the benzylic and the methylenic protons of the S(61,2) SO adduct and the adjacent DNA oriented the styrene ring within the major groove (Figure 4). The styrene phenyl protons interacted with C^{15},T^{16}, and T^{17} major groove protons in the complementary strand, oriented on the 3′-side of the modified site. The methylenic protons and the benzylic proton interacted with C^5 major groove protons of the modified strand, oriented on the 5′-side of the modified site. The second-order NOEs between styrene phenyl protons and C^5 H5, H6, and N4$H_{a,b}$ suggested that although the phenyl ring of styrene was oriented toward the 3′-side of the modified strand, it was situated between the C^5·G^{18} and A^7·T^{16} base pairs.

The S(61,3) adduct also adopted a solution conformation in the B-family with modest structural perturbations at and adjacent to the lesion site. The styrene ring was oriented edgewise such that it was approximately orthogonal to the edge of the C^{15} pyrimidine ring. Base-pairing interactions remained intact at the site of the lesion, consistent with the NMR data for the imino protons (Figure 2C). The styrenyl aromatic protons interacted with major groove protons of T^{14}, C^{15}, and T^{16} in the complementary strand, with H_b and CH_2OH interacted with A^6 and $^{S\text{-}SO}A^7$ major groove protons in the modified strand.

The structure refined from NOE data (Figure 8) was corroborated by chemical shift perturbations. Protons in the major groove and located on the 3′-side of the adduct in the modified strand underwent increased shielding, which was consistent with the predicted location of the styrene aromatic ring. This effect was particularly pronounced for C^{15} N4H_a, which shifted upfield 2.6 ppm. C^{15} H5 was likewise shifted,

A

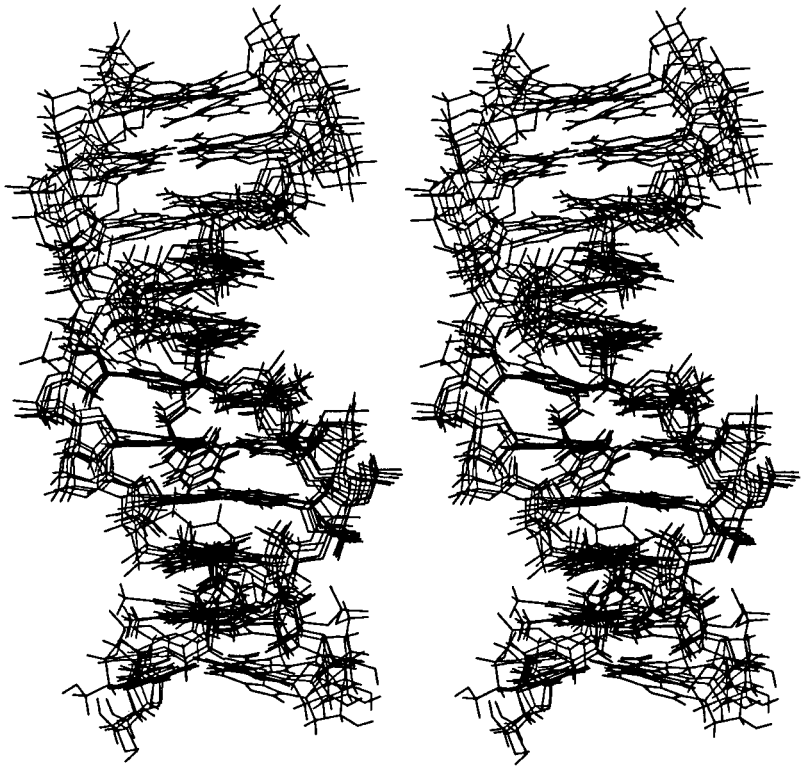

<rMDA>

B

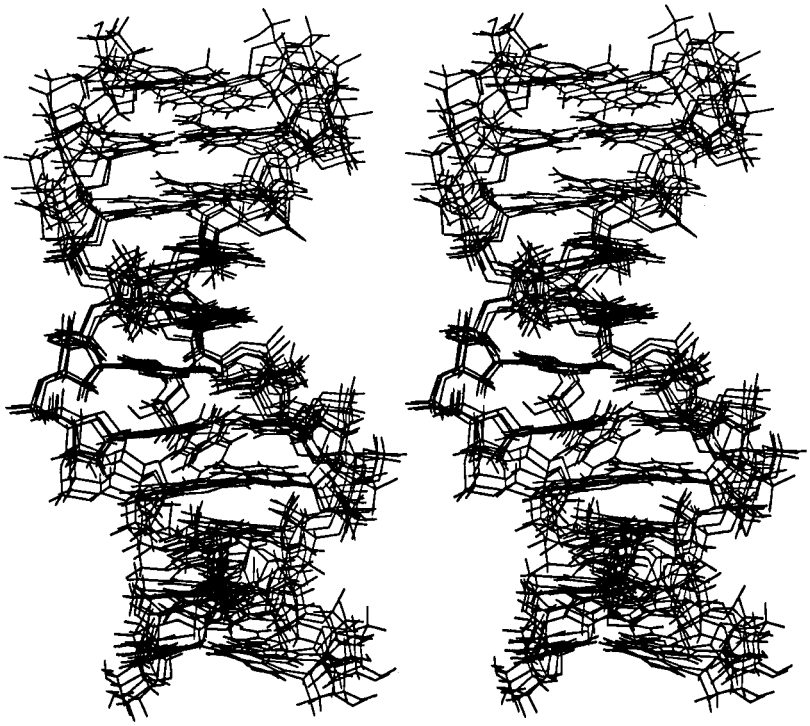

<rMDB>

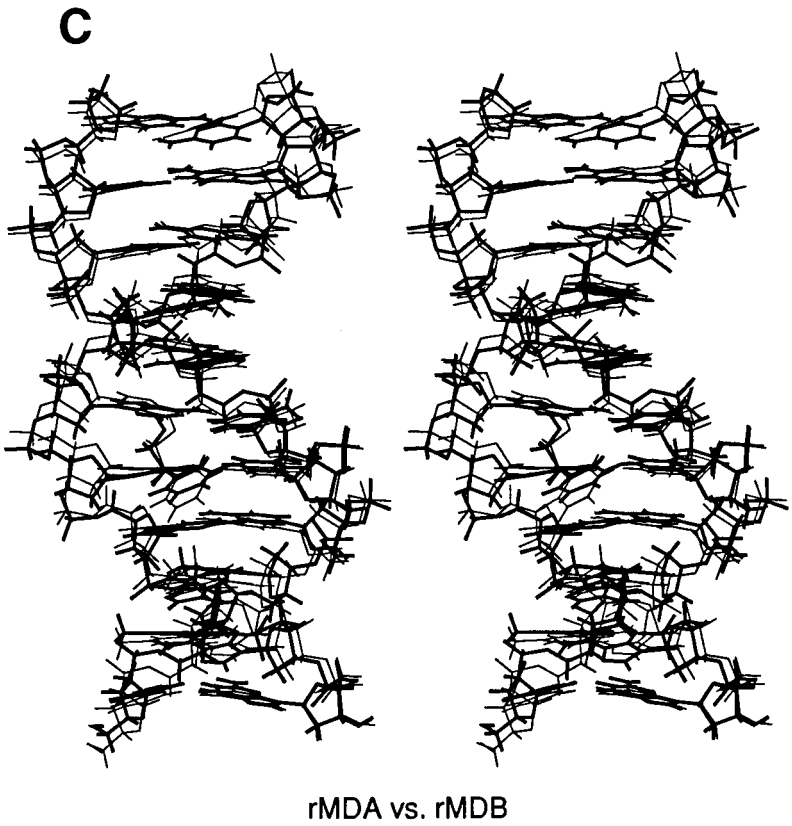

FIGURE 6: For the S(61,3) adduct, stereo drawings of (A) five MD structures which emerged from calculations using IniA as the starting structure, (B) five MD structures which emerged from calculations using IniB as the starting structure, and (C) the superposition of the rMDA and rMDB structure. The structure drawn in bold is that of rMDB.

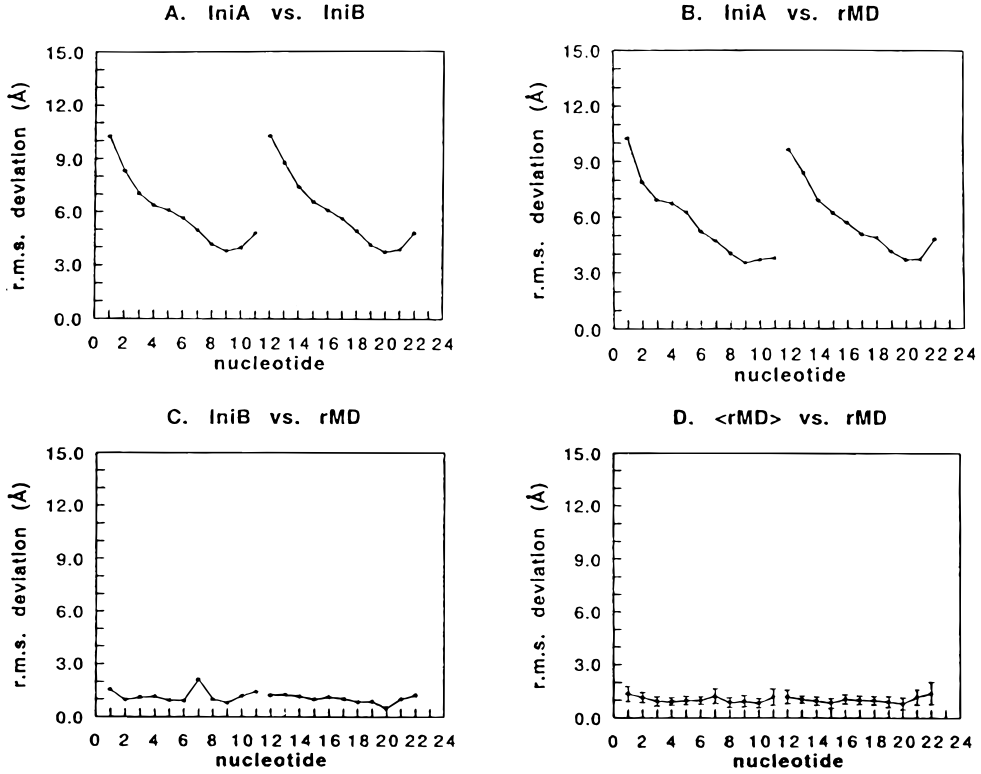

FIGURE 7: Per residue rmsd comparisons between the initial structures and the final structures for the S(61,3) adduct. (A) Comparison of IniA vs IniB. (B) Comparison of IniA vs rMD. (C) Comparison of IniB vs rMD. (D) ⟨rMD⟩ vs rMD is the comparison of each of the final structures with the energy-minimized average of the 10. The error bars represent the standard deviation observed at each nucleotide.

0.5 ppm upfield. Unexpectedly large changes were noted for A^{6} H1′ and $^{S\text{-}SO}A^{7}$ H1′, which shifted downfield 0.3 and upfield 0.2 ppm, respectively. These perhaps indicate alterations in base stacking orientation of the $A^{6}\cdot T^{17}$ and $^{S\text{-}SO}A^{7}\cdot T^{16}$ base pairs which would bring the respective H1′ protons either under greater or lesser influence of ring current interactions. The MD calculations suggested the potential for hydrogen bond formation in the S(61,3) adduct, between

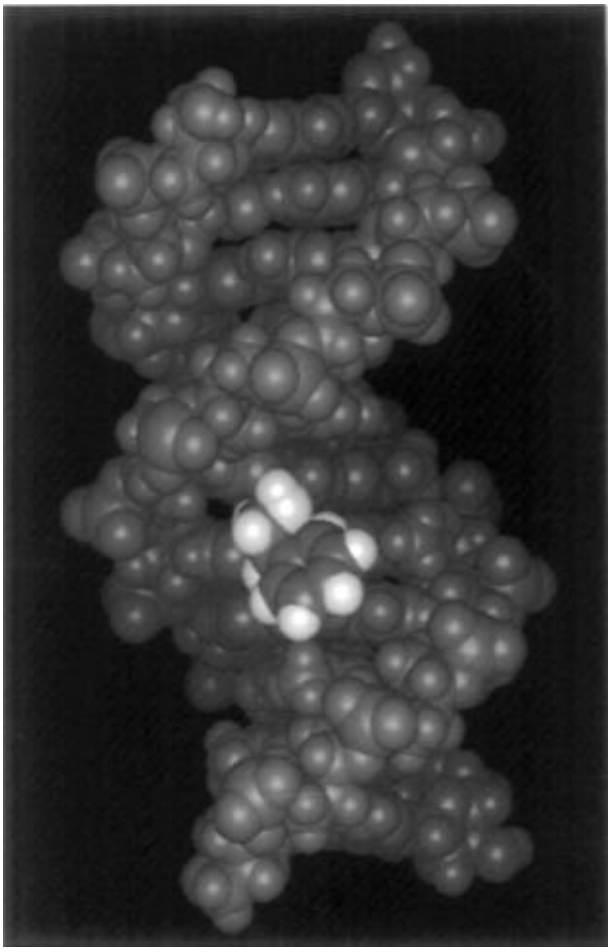

FIGURE 8: CPK representation of the final MD structure of the S(61,3) adduct. SO is shown in blue. Protons on SO are shown in white. This model structure is based upon averaging the coordinates from 10 MD calculations (see text).

Table 2: Comparison of Sixth Root Residual Indices R_1^x for Starting Models and Resulting MD Structures as a Function of NOE Mixing Time for the S(61,3) Adduct[a]

	R_1^x ($\times 10^{-2}$)		
structure	$t_m = 150$ ms	$t_m = 200$ ms	$t_m = 250$ ms
IniA	16	16	16
IniB	11	12	11
rMDA	9.6	9.7	9.4
rMDB	9.6	9.7	9.4
rMD_{final}	9.4	9.5	9.2

[a] Only the inner nine base pairs were used in the calculations to exclude end effects. $R_1^x = \sum|(a_o)_i^{1/6} - (a_c)_i^{1/6}|/\sum|(a_o)_i^{1/6}|$, where ($a_o$) and ($a_c$) are the intensities of observed (non-zero) and calculated NOE cross-peaks. Abbreviations: IniA, starting energy-minimized A-DNA; IniB, starting energy-minimized B-DNA; rMDA, average of five rMD structures starting from IniA; rMDB, average of five MD structures starting from IniB; rMD_{final}, average of ten MD structures starting from IniA and IniB.

the hydroxyl group of SO and A^6 N7, of the neighboring base pair in the 5′-direction. This was not observed, perhaps because of exchange with solvent.

Stereochemistry Effects. A comparison of the S(61,2) (major conformation) and S(61,3) adducts with the diastereomeric R(61,2) and R(61,3) adducts (Feng et al., 1995) revealed that the SO moiety was also accommodated in the major groove for the two (*S*)-α-styrene oxide adducts but the orientation of the styrenyl moiety was reversed. For the *S* diastereomers, the phenyl rings were oriented toward the 3′-direction from the site of adduction, while for the *R* diastereomers, the phenyl rings were oriented toward the 5′-direction. The relationship between the orientation of the phenyl ring and the stereochemistry of the benzylic carbon was consistent for both SO adducts and PAH adducts located at adenine N6. The (+)-(1*R*)-benzo[*c*]phenanthrene adduct and the (−)-(7*S*,8*R*,9*S*,10*R*)- and (−)-(7*R*,8*S*,9*S*,10*R*)-benzo[*a*]pyrene adducts (Cosman et al., 1993; Schurter et al., 1995a,b; Zegar et al, 1996) had the same stereochemistry as the R(61,2) and R(61,3) SO adducts. In each instance, the adducts were oriented toward the 5′-direction. In contrast, for the (−)-(1*S*)-benzo[*c*]phenanthrene (Cosman et al., 1995) and the S(61,2) and S(61,3) SO adducts, the phenyl rings faced toward the 3′-side of the modified site. The key difference between adenine N6 PAH adducts and the SO adducts was the intercalation of the PAH adducts (Cosman et al., 1993, 1995; Schurter et al., 1995a,b; Zegar et al., 1996), while the SO adducts were in the groove. Perhaps this reflects the greater propensity for the PAH aromatic ring system to intercalate. The facile rotation of the styrene ring, compared to PAH adducts which do not undergo rotation, might also inhibit intercalation of SO. For both the major conformation of the S(61,2) adduct and for the S(61,3) adduct, the rates of aromatic ring flips were fast on the NMR time scale (Wuthrich & Wagner, 1978). This contrasted with the slower (NMR time scale) rate of ring flips observed for the R(61,2) and R(61,3) adducts (Feng et al., 1995). It was consistent with the lack of steric constraints toward ring flips in the major groove for the *S* adducts, whereas for the *R*

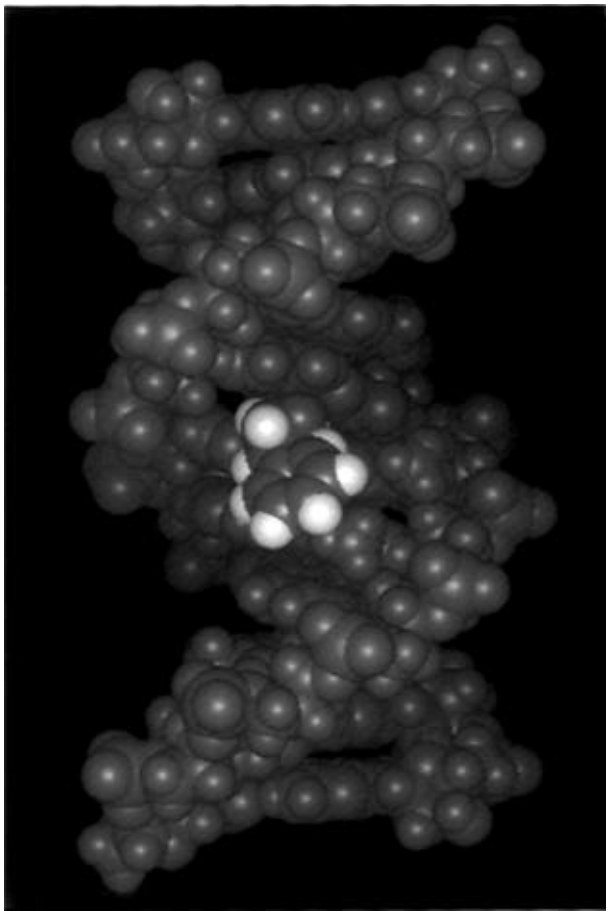

FIGURE 9: Calculated structure from molecular mechanics for the S(61,2) adduct indicating that the styrene moiety is oriented in the major groove pointing toward the 3′-side of the modified site.

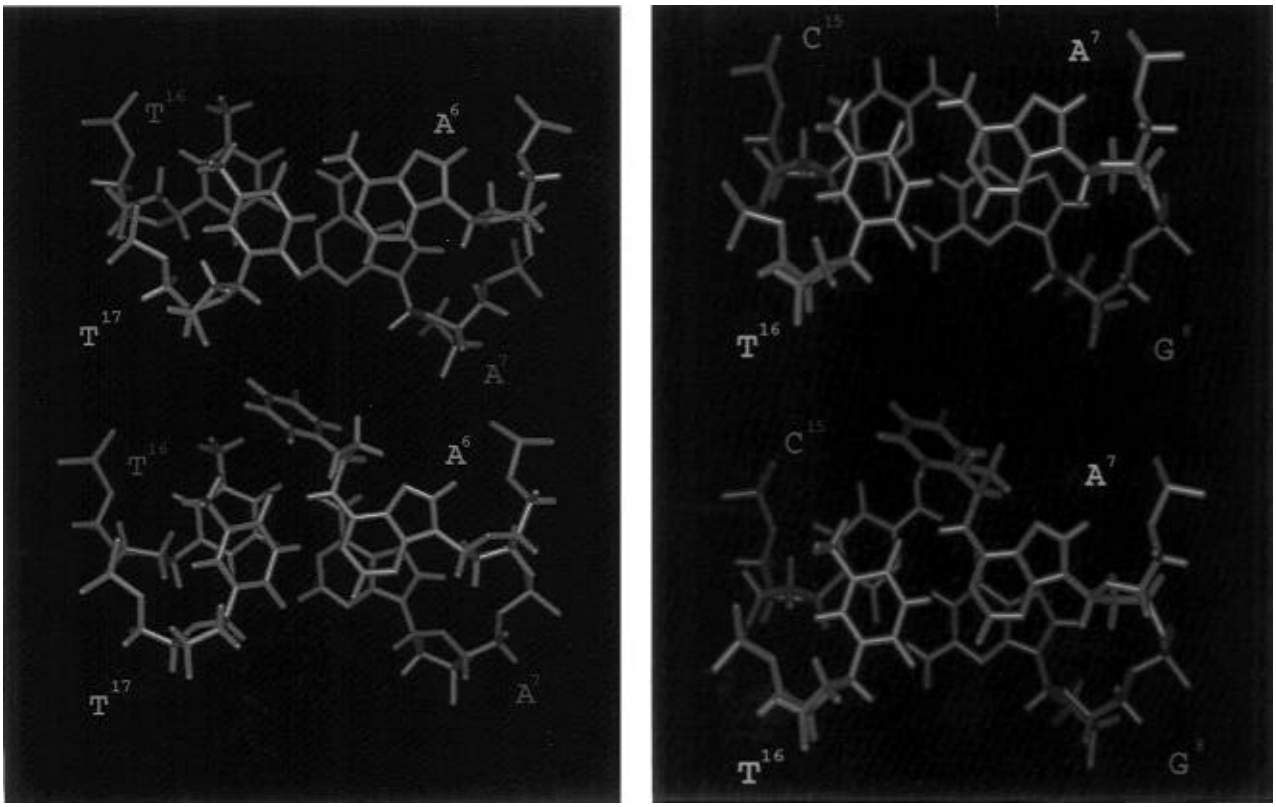

FIGURE 10: (A, left) Comparison of stacking patterns of the $A^6 \cdot T^{17}$ base pair above $A^7 \cdot T^{16}$ in the unmodified *ras61* oligodeoxynucleotide (top panel) and $^{S\text{-}SO}A^6 \cdot T^{17}$ above $A^7 \cdot T^{16}$ in the S(61,2) oligodeoxynucleotide (bottom panel). (B, right) Comparison of stacking patterns of the $A^7 \cdot T^{16}$ base pair above $G^8 \cdot C^{15}$ in the unmodified *ras61* oligodeoxynucleotide (top panel) and $^{S\text{-}SO}A^7 \cdot T^{16}$ above $G^8 \cdot C^{15}$ in the S(61,3) oligodeoxynucleotide (bottom panel).

diastereomers, the styrene ring crowded the 5′-neighbor base pair in the major groove (Feng et al., 1995).

Sequence Effects. One surprise was the large sequence effect observed for the S(61,2) and S(61,3) sequence isomers, as compared to the R(61,2) and R(61,3) sequence isomers which showed smaller changes in conformation (Feng et al., 1995). The observation of two conformations for the S(61,2) adduct but a single conformation of the S(61,3) adduct provides a striking example of the importance of DNA sequence context in understanding adduct properties. Conformational equilibria are a feature of a number of DNA adducts (Cho et al., 1992, 1994; Eckel & Krugh, 1994a,b). The role of such equilibria in modulating biological outcome remains to be established. In the *ras61* sequence, the S(61,2) adduct was not strongly mutagenic in repair-deficient bacterial systems (Latham et al., 1993). Interconversion between two adduct conformations has been described as a "mutagenic switch" (Eckel & Krugh, 1994a,b). Other adducts equilibrate between multiple conformations, including propanodeoxyguanosine (Singh et al., 1993), aminofluorene (Cho et al., 1994; Eckel & Krugh, 1994a,b), and benzo[*a*]pyrene (Rodriguez & Loechler, 1993a,b). This phenomenon shows the importance of DNA sequence and illustrates the complexities of correlating adduct structure with function. Furthermore, it is important to consider that the structures obtained in this study represent equilibrium conformations. The degree to which they are representative of transient intermediates formed during replication or repair (Randall et al., 1987; Singer et al., 1989; Voigt & Topal, 1990; Rodriguez & Loechler, 1993b) is not known.

Biological Implications. The S(61,2) and S(61,3) adducts examined in this work provide useful model systems for the stereochemical consequences of SO adduction at adenine N6, within a DNA sequence in which mutagenesis is expected to activate the *n-ras* protooncogene. The functional significance of the S(61,2) and S(61,3) SO adducts with regard to human carcinogenesis remains to be established. Concerns regarding styrene toxicity are due to the wide utilization of styrene in the chemical manufacturing industry and its reported mutagenicity in various cell lines, including those from humans (Ott et al., 1980; Hodgson & Jones, 1985; Matanoski & Schwarts, 1987; Wong, 1990). SO adducts can be detected and examined *in vitro*, but the adduct spectrum in human cells has not been characterized.

The polycyclic aromatic hydrocarbon dimethylbenz[*a*]anthracene was implicated as a causal factor in point mutations at codon 61 (Quintanilla et al., 1986; Bizub et al., 1986), as was the arylamine *N*-hydroxy-2-(acetylamino)fluorene (Wiseman et al., 1986). The recent report that rat *h-ras* mutants in codon 12 widely believed to have arisen from nitrosomethylurea (Zarbl et al., 1985) may have arisen spontaneously during pubertal growth of the mammary gland and were not induced by nitrosomethylurea (Cha et al., 1994) illustrates the need to demonstrate a direct linkage between adduction in the codon 61 sequence and subsequent mutagenesis. Nevertheless, it seems likely that electrophilic species such as SO can form adducts in the codon 61 sequence, which provide one potential avenue toward the induction of activating mutations.

One factor which may contribute toward determining the fate of potential SO adenine N6 adducts is the ability of replication complexes to bypass the damage site. Primer extension using bacterial and eukaryotic polymerases revealed that templates bearing the S(61,2) and S(61,3) SO

adducts were replicated differently (Latham et al., 1995). This suggested that sequence-specific changes in adduct structure such as have been revealed in the present work could play a role in the by-pass of these lesions. The primer extension studies also suggested polymerase-specific differences in the mechanisms by which these adducts were processed by the enzymes. A long-range goal is to correlate conformational differences among these different diastereomers with biochemical studies (Latham et al., 1993, 1995; Latham & Lloyd, 1994).

Summary. Two sequence isomeric (*S*)-α-styrene oxide adducts at adenine N6 in the *ras61* coding sequence revealed the influence of stereochemistry and DNA sequence upon adduct structure. As compared to the (*R*)-α-styrene oxide adducts at these same loci, the *S* adducts were oriented in the major groove in the opposite direction, having the styrenyl rings facing the 3′-direction from the site of the lesion, and underwent rapid ring flips. A strong sequence effect was observed, with the S(61,2) adduct equilibrating between two conformations and the S(61,3) adduct forming a single major groove structure.

ACKNOWLEDGMENT

Drs. James G. Moe and Irene S. Zegar and Mr. Jason P. Weisenseel assisted with NMR spectroscopy and structural refinement. Mr. Gary J. Latham and Professor R. Stephen Lloyd (The University of Texas Medical Branch, Galveston) provided helpful discussions. We thank Dr. Ed Mooberry and the NMRFAM, Madison, WI, for assistance with 750 MHz NMR spectra. We thank Dr. Hui Mao for assistance with preparation of the manuscript.

SUPPORTING INFORMATION AVAILABLE

Tables S1−S5, which detail the ^{1}H NMR chemical shift assignments for the S(61,2) and S(61,3) adducts and the experimental distances and classes of restraints for the S(61,3) oligodeoxynucleotide (13 pages). Ordering information is given on any current masthead page.

REFERENCES

Balmain, A., & Brown, K. (1988) *Adv. Cancer Res. 51*, 147−182.
Barbacid, M. (1987) *Annu. Rev. Biochem. 56*, 779−827.
Bax, A., Sklenar, V., & Clore, G. M. (1987) *J. Am. Chem. Soc. 109*, 6511−6513.
Bizub, D., Wood, A. W., & Skalka, A. M. (1986) *Proc. Natl. Acad. Sci. U.S.A. 83*, 6048−6052.
Bodenhausen, G., Kogler, H., & Ernst, R. R. (1984) *J. Magn. Reson. 58*, 370−388.
Boelens, R., Scheek, R. M., Dijkstra, K., & Kaptein, R. (1985) *J. Magn. Reson. 62*, 378−386.
Bonatti, S., Abbondandolo, A., Corti, G., Fiorio, R., & Mazzaccaro, A. (1978) *Mutat. Res. 52*, 295−300.
Bond, J. A. (1989) *CRC Crit. Rev. Toxicol. 19*, 227−249.
Borer, P. N. (1975) in *Handbook of Biochemistry and Molecular Biology*, CRC Press, Cleveland, OH.
Borgias, B. A., & James, T. L. (1990) *J. Magn. Reson. 87*, 475−487.
Brooks, B. R., Bruccoleri, R. E., Olafson, B. D., States, D. J., Swaminathan, S., & Karplus, M. (1983) *J. Comput. Chem. 4*, 187−217.
Brunger, A. T. (1992) In *X-PLOR. Version 3.1. A System for X-ray Crystallography and NMR*, Yale University Press, New Haven, CT.
Calladine, C. R. (1982) *J. Mol. Biol. 161*, 343−352.
Cha, R. S., Thilly, W. G., & Zarbl, H. (1994) *Proc. Natl. Acad. Sci. U.S.A. 91*, 3749−3753.
Cho, B. P., Beland, F. A., & Marques, M. M. (1992) *Biochemistry 31*, 9587−9602.
Cho, B. P., Beland, F. A., & Marques, M. M. (1994) *Biochemistry 33*, 1373−1384.
Cosman, M., Fiala, R., Hingerty, B. E., Laryea, A., Lee, H., Harvey, R. G., Amin, S., Geacintov, N. E., Broyde, S., & Patel, D. (1993) *Biochemistry 32*, 2488−2497.
Cosman, M., Laryea, A., Fiala, R., Hingerty, B. E., Amin, S., Geacintov, N. E., Broyde, S., & Patel, D. J. (1995) *Biochemistry 34*, 1295−1307.
de Meester, C., Poncelet, F., Roberfroid, M., Rondelet, J., & Mercier, M. (1977) *Mutat. Res. 56*, 147−152.
Eckel, L. M., & Krugh, T. R. (1994a) *Nat. Struct. Biol. 1*, 89−94.
Eckel, L. M., & Krugh, T. R. (1994b) *Biochemistry 33*, 13611−13624.
Elovaara, E., Engstrom, K., Nakajima, T., Park, S. S., Gelboin, H. V., & Vainio, H. (1991) *Xenobiotica 21*, 651−661.
Feng, B., & Stone, M. P. (1995) *Chem. Res. Toxicol. 8*, 821−832.
Feng, B., Zhou, L., Passarelli, M., Harris, C. M., Harris, T. M., & Stone, M. P. (1995) *Biochemistry 34*, 14021−14036.
Foureman, G. L., Harris, C., Guengerich, F. P., & Bend, J. R. (1989) *J. Pharmacol. Exp. Ther. 248*, 492−497.
Guengerich, F. P. (1992) *FASEB J. 6*, 745−748.
Guengerich, F. P., Kim, D.-H., & Iwasaki, M. (1991) *Chem. Res. Toxicol. 4*, 168−179.
Harris, C., Philpot, R. M., Hernandez, O., & Bend, J. R. (1986) *J. Pharmacol. Exp. Ther. 236*, 144−149.
Harris, C. M., Zhou, L., Strand, E. A., & Harris, T. M. (1991) *J. Am. Chem. Soc. 113*, 4328−4329.
Havel, T. F., & Wuthrich, K. (1985) *J. Mol. Biol. 182*, 281−294.
Hodgson, J. T., & Jones, P. D. (1985) *J. Work Environ. 11*, 347−352.
Keepers, J. W., & James, T. L. (1984) *J. Magn. Reson. 57*, 404−426.
Latham, G. J., & Lloyd, R. S. (1994) *J. Biol. Chem. 269*, 28527−28530.
Latham, G. J., Zhou, L., Harris, C. M., Harris, T. M., & Lloyd, R. S. (1993) *J. Biol. Chem. 268*, 23427−23434.
Latham, G. J., Harris, C. M., Harris, T. M., & Lloyd, R. S. (1995) *Chem. Res. Toxicol. 8*, 422−430.
Madrid, M., Llinas, E., & Llinas, M. (1991) *J. Magn. Reson. 93*, 329−346.
Marion, D., Ikura, M., & Bax, A. (1989) *J. Magn. Reson. 84*, 425−430.
Matanoski, G. M., & Schwarts, L. (1987) *J. Occup. Med. 29*, 675−680.
Miller, E. C. (1978) *Cancer Res. 38*, 1479−1496.
Miller, J. A. (1970) *Cancer Res. 30*, 559−576.
Mujeeb, A., Kerwin, S. M., Kenyon, G. L., & James, T. L. (1993) *Biochemistry 32*, 13419−13431.
Nakajima, T., Elovaara, E., Gonzalez, F. J., Gelboin, H. V., Raunio, H., Pelkonen, O., Vainio, H., & Aoyama, T. (1994a) *Chem. Res. Toxicol. 7*, 891−896.
Nakajima, T., Wang, R.-S., Elovaara, E., Gonzalez, F. J., Gelboin, H. V., Vainio, H., & Aoyama, T. (1994b) *Biochem. Pharmacol. 48*, 637−642.
Nelson, D. R., Kamataki, T., Waxman, D. J., Guengerich, F. P., Estabrook, R. W., Feyereisen, R., Gonzalez, F. J., Coon, M. J., Gunsalus, I. C., Goto, O., Okuda, K., & Nebert, D. W. (1993) *DNA Cell Biol. 10*, 1−51.
Nilsson, L., & Karplus, M. (1986) *J. Comput. Chem. 7*, 591−616.
Nilsson, L., Clore, G. M., Gronenborn, A. M., Brunger, A. T., & Karplus, M. (1986) *J. Mol. Biol. 188*, 455−475.
Norppa, H., Sorsa, M., Pfaffli, P., & Vainio, H. (1980) *Carcinogenesis 1*, 357−361.
Norppa, H., Hemminki, K., Sorsa, M., & Vainio, H. (1981) *Mutat. Res. 91*, 243−250.
Ott, M. G., Kolesar, R. C., Schamweber, H. C., Schneider, E. J., & Venable, J. R. (1980) *J. Occup. Med. 22*, 445−460.
Plateau, P., & Gueron, M. (1982) *J. Am. Chem. Soc. 104*, 7310−7311.
Quintanilla, M., Brown, K., Ramsden, M., & Balmain, A. (1986) *Nature 322*, 78−80.
Randall, S. K., Eritja, R., Kaplan, B. E., Petruska, J., & Goodman, M. F. (1987) *J. Biol. Chem. 262*, 6864−6870.

Ravishankar, G., Swaminathan, S., Beveridge, D. L., Lavery, R., & Sklenar, H. (1989) *J. Biomol. Struct. Dyn. 6*, 669−699.
Rodriguez, H., & Loechler, E. L. (1993a) *Carcinogenesis 14*, 373−383.
Rodriguez, H., & Loechler, E. L. (1993b) *Biochemistry 32*, 1759−1769.
Ryckaert, J.-P., Ciccotti, G., & Berendsen, H. J. C. (1977) *J. Comput. Phys. 23*, 327−341.
Savela, K., & Hemminki, K. (1986) *Arch. Toxicol., Suppl. 9*, 281−285.
Schurter, E. J., Sayer, J. M., Oh-hara, T., Yeh, H. J. C., Yagi, H., Luxon, B. A., Jerina, D. M., & Gorenstein, D. G. (1995a) *Biochemistry 34*, 9009−9020.
Schurter, E. J., Yeh, H. J. C., Sayer, J. M., Lakshman, M. K., Yagi, H., Jerina, D. M., & Gorenstein, D. G. (1995b) *Biochemistry 34*, 1364−1375.
Singer, B., Chavez, F., Goodman, M. F., Essigmann, J. M., & Dosanjh, M. K. (1989) *Proc. Natl. Acad. Sci. U.S.A. 86*, 8271−8274.
Singh, U. S., Moe, J. G., Reddy, G. R., Weisenseel, J. P., Marnett, L. J., & Stone, M. P. (1993) *Chem. Res. Toxicol. 6*, 825−836.
Sklenar, V., Brooks, B. R., Zon, G., & Bax, A. (1987) *FEBS Lett. 216*, 249−252.
Voigt, J. M., & Topal, M. D. (1990) *Biochemistry 29*, 5012−5018.
Wade, D. R., Airy, S. C., & Sinsheimer, J. E. (1978) *Mutat. Res. 58*, 217−223.
Weisz, K., Shafer, R. H., Egan, W., & James, T. L. (1994) *Biochemistry 33*, 354−366.
Wiseman, R., Stowers, S., Miller, E., Anderson, M., & Miller, J. (1986) *Proc. Natl. Acad. Sci. U.S.A. 83*, 5285−5289.
Wong, O. (1990) *J. Ind. Med. 47*, 753−762.
Wuthrich, K. (1986) in *NMR of Proteins and Nucleic Acids*, John Wiley & Sons, New York.
Wuthrich, K., & Wagner, G. (1978) *Trends Biochem. 3*, 227−230.
Zarbl, H., Sukumar, S., Arthuyr, A. V., Martin-Zanca, D., & Barbacid, M. (1985) *Nature 315*, 382−385.
Zegar, I. S., Kim, S. J., Johansen, T. N., Horton, P. J., Harris, C. M., Harris, T. M., & Stone, M. P. (1996) *Biochemistry 35*, 6212−6224.

BI952526F